Numerical study of the effects of strain rate on the behaviour of dynamically penetrating anchors in clay

***H. Sabetamal[1], J. P. Carter[1], M. Nazem[2] and S.W. Sloan[1]**

[1] ARC Centre of Excellence for Geotechnical Science and Engineering, The University of Newcastle, NSW, Australia.

[2] School of Engineering, RMIT University, Melbourne, Australia

*Presenting author: Hassan.sabetamal@uon.edu.au

*Corresponding author: Hassan.sabetamal@uon.edu.au

Abstract

The installation of torpedo anchors at high impact velocities imposes high strain rates in the surrounding soil. The high strain rates enhance the mobilised undrained shear strength compared to that measured statically by laboratory or in situ tests. To illustrate the implications of such high strain rates for the behaviour of dynamic anchors, large deformation Finite Element (FE) analyses were carried out. The numerical FE scheme is based on a dynamic coupled effective stress framework with the Modified Cam Clay constitutive model. The soil constitutive model is adapted to incorporate the dependence of clay behaviour on strain rata. In order to assess the validity of the numerical scheme, some laboratory tests on model free falling penetrometers have been simulated. The results indicate that overall the agreement between computations and measurements is good. It is seen that the generation of excess pore pressure around dynamically installed anchors and the frictional resistance at the soil-anchor interface are significantly affected by the strain rate. Moreover, increased strain rate dependency of the soil leads to a marked reduction in the embedment depth, reflecting a noticeable increase in the soil penetration resistance.

Keywords: Torpedo anchors, Strain rate dependency, Dynamic coupled analysis, Large deformations.

Introduction

Deepwater oil and gas reserves have become an important component of global energy supply, and the recovery of hydrocarbons from these regions has resulted in a broad range of relatively new engineering practices. The scale of the foundation and anchoring elements, along with their novel construction and installation techniques, are key aspects of offshore geotechnical engineering. Depending on the depth of the seabed, offshore structures may be divided into two main types: fixed and floating structures. All floating systems used in deep waters require moorings and ultimately some form of anchor on the seabed, which typically include surface (gravity) and embedded anchors. Dynamically installed anchors (*i.e.*, torpedo anchors and deep penetrating anchors) are promising embedment systems used in ultra-deep waters, mainly due to their installation cost advantage compared to other systems such as drag embedment anchors and suction embedded plate anchors. A torpedo anchor is embedded using the kinetic energy attained by gravity free fall through the water column, so that its installation cost is largely independent of water depth. This anchoring system also has a relatively lower fabrication cost which often makes it more attractive than suction caissons.

Despite the economic advantages afforded by dynamically installed anchors, there remain significant uncertainties in the prediction of the embedment depth and the anchor holding capacity. The prediction of the embedment depth is complicated by the very high strain rate adjacent to the soil-anchor interface (resulting from high penetration velocities) and hydrodynamic aspects which can involve inertial and viscous drag forces.

It is well known that the mechanical behaviour of clayey soil is affected by the rate of induced strains. Typically, the undrained strength increases with increasing shear strain rate (e.g., [1]-[5]). Therefore, for high velocity penetrations, the soil resistance under fully undrained conditions might be expected to vary as a function of the strain rate. Numerical studies have actually shown that the effect of the strain rate on the shear strength of the soil should not necessarily be ignored in problems involving the fast penetration of objects into soil layers (*e.g.*, [6][7]). However, there is a lack of knowledge on how the excess pore pressures and frictional forces at the anchor-soil interface might be affected by strain rate effects.

Sabetamal *et al.* [9][10] presented rigorous coupled analyses for a few free falling torpedo anchors. These initial studies reported successful simulations of the installation process and reconsolidation stage of torpedo anchors, and revealed the pattern in which excess pore pressures are generated and dissipated. In this paper, we extend our earlier study to capture the effects of strain rate on the behaviour of torpedo anchors. Accordingly, some numerical findings are reported on the performance of this anchoring system during the installation phase, taking both the strain rate and inertial drag forces into account.

Numerical Scheme

Problems in offshore geomechanics are typically characterized by the existence of hydrodynamic and cyclic loadings, large deformations, extreme soil-structure interactions and soil disturbance typically due to installation effects. The installation of offshore structures, such as a dynamically embedded anchor, is usually an undrained process during which excess pore pressures are generated. The time scale of consolidation is also important for predicting the holding capacity of these anchors under different loading events. A fully coupled analysis is then required to incorporate pore-fluid pressure development and its subsequent dissipation.

Governing equations

A continuum approach based on the theory of mixtures [11] and the concept of volume fractions [12] is employed to derive the governing equations. Sabetamal [13] provided a detailed account of the governing differential equations and the corresponding weak statements that form the basis of our finite element (FE) modelling. A mixed formulation were selected to describe both incompressible and compressible fluids, in which the resulting formulation predicts all field variables, including the solid matrix displacements **U**, pore-fluid pressure **P**, and Darcy velocity of the pore fluid $\mathbf{V}_r$. The resulting equation system governing the behaviour of the soil-water mixture may be written in matrix form as

$$\begin{bmatrix} \mathbf{M}_{ss} & 0 & \mathbf{M}_{sr} \\ 0 & 0 & 0 \\ \mathbf{M}_{rs} & 0 & \mathbf{M}_{rr} \end{bmatrix} \begin{bmatrix} \ddot{\mathbf{U}} \\ \ddot{\mathbf{P}} \\ \dot{\mathbf{V}}_r \end{bmatrix} + \begin{bmatrix} \mathbf{C}_s & 0 & 0 \\ \mathbf{C}_{ps} & -\mathbf{C}_{pr} & \mathbf{C}_{pp} \\ 0 & \mathbf{C}_{rr} & 0 \end{bmatrix} \begin{bmatrix} \dot{\mathbf{U}} \\ \dot{\mathbf{P}} \\ \mathbf{V}_r \end{bmatrix} + \begin{bmatrix} \mathbf{K}_\sigma & \mathbf{K}_{sp} & 0 \\ 0 & \mathbf{K}_{rp} & 0 \\ 0 & \mathbf{K}_{pp} & 0 \end{bmatrix} \begin{bmatrix} \mathbf{U} \\ \mathbf{P} \\ \mathbf{0} \end{bmatrix} = \begin{bmatrix} \mathbf{F}^s \\ \mathbf{F}^p \\ \mathbf{F}^r \end{bmatrix} \quad (1)$$

where $\mathbf{M}_{ss}, \mathbf{M}_{rr}, \mathbf{M}_{rs} = \mathbf{M}_{sr}^{T}$ and $\mathbf{C}_{\alpha\beta}$ are the solid mass, fluid mass, coupled fluid mass and damping matrices, respectively. $\mathbf{K}_{\sigma}$ and $\mathbf{K}_{pp}$ are, respectively, the stiffness and compressibility matrices while $\mathbf{K}_{\alpha\beta}$ represent coupling matrices and $\mathbf{F}^{s}, \mathbf{F}^{p}$ and $\mathbf{F}^{r}$ are the vectors of external nodal forces.

Large deformation and mesh refinement

To consider large deformation phenomena and avoid possible mesh distortions, the traditional numerical methods established within a Lagrangian framework are typically replaced by those based on the framework of the Arbitrary Lagrangian Eulerian (ALE) method. ALE approaches for geotechnical applications can be divided into two groups: mesh based methods [14]-[17] and particle based schemes such as the material point method [18][19]. The mesh based ALE schemes used in geotechnical engineering may be divided into three categories: the Remeshing and Interpolation Technique involving Small Strains (RITSS) [15], the ALE scheme [20], and the Coupled Eulerian-Lagrangian (CEL) approach. Wang *et al.* [21] compared the performances of the three approaches for some benchmark problems covering static, consolidation and dynamic geotechnical applications. It was concluded that the RITTS and ALE schemes predict close results whereas, for dynamic problems, the results obtained from the CEL approach differ from those predicted with the RITTS and ALE methods. The ALE scheme [17] is incorporated in this study to handle large deformations. In this approach, some special care should be taken for the solution of the advection equations, where transport of the material and the current solution state through the mesh is considered along the streamlines of the advective flow, provided by the convective velocity. In an ALE framework, this corresponds to a relocation of the FE nodes by the mesh motion scheme, while the material is held fixed in space. Most advection schemes, especially the classical first-order methods, show highly numerical diffusive properties. This appears to be crucial for the cases that hardening/softening is involved in the solution by some constitutive models such as the Modified Cam Clay (MCC) model. The transport step has to be then split into multiple advection steps, based on intermediate mesh configurations, and an advection scheme with only a small amount of diffusion is necessary to retain the special shape of the solution variables properly [22].

Interface modelling

The so called one pass node-to-segment (NTS) discretisation method is commonly used to analyse large sliding and large deformation problems of contact mechanics [23][24]. Sabetamal *et al.* [10] applied the NTS scheme to analyse some coupled dynamic problems and observed that smooth discretisation of the contact interface between soil and structure is a crucial factor to avoid severe oscillations in the predicted dynamic forces and pore fluid pressures. It is also noted that a consistent coupling of the NTS contact with elements of a higher order is not possible because contact constraints are only fulfilled locally at a number of finite connection points. In contrast, the mortar segment-to-segment approach [24][25] considers the enforcement of contact constraints in a weak integral form so that high-order approximation functions can be used to interpolate different field variables. The use of high order elements also provides the possibility to explicitly incorporate smooth continuous geometries in the FE model, thus avoiding the numerical oscillations encountered in NTS approach. Sabetamal *et al.* [26] developed and applied a frictionless mortar scheme to model some dynamic problems of two phase saturated problems. In this paper, we use an extended form of the scheme which can also model frictional interfaces embedded within two phase saturated porous media [13].

Strain rate effect

The dependence of undrained shear strength of soil on applied rate of strain has long been recognized [27] and studied extensively both in triaxial compression tests (e.g., [28][3]) and vane shear tests (e.g., [29][4]). The dependence of shear strength s_u on strain rate $\dot{\gamma}$ maybe characterised in terms of a semi-logarithmic relation [1]

$$s_u = s_{u_{ref}} \left[1 + \eta \log \left(\frac{\dot{\gamma}}{\dot{\gamma}_{ref}} \right) \right] \tag{2}$$

where $s_{u_{ref}}$ is the reference undrained shear strength measured at the reference strain rate $\dot{\gamma}_{ref}$ and η denotes the rate of increase per decade with a suggested range of 0.05 to 0.20. In this study, the nonlinear behaviour of the solid constituent in the two phase saturated mixture is captured by the MCC soil model. Typical undrained strain rates in standard laboratory tests measure around 0.01/h (3×10^{-6} s^{-1}). Assuming this rate as the reference strain rate, the initial undrained shear strength predicted by the constitutive model parameters will correspond to $s_{u_{ref}}$. Fig. 1 depicts the locus of normal consolidation line (*NCL*) and overconsolidation line in v-ln(p') space for an overconsolidated soil (v_i, p'_i), where v_i denotes specific volume, p' is mean effective stress, N is the value of specific volume at unit pressure, λ is the slope of the *NCL*, κ represents the slope of unloading-reloading line and q is deivatoric stress.

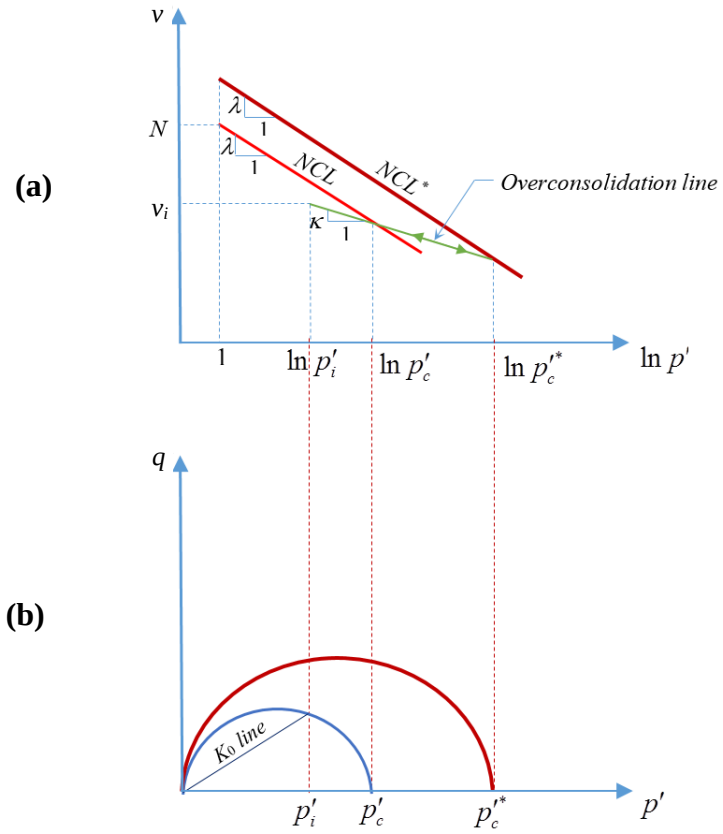

Figure 1. (a) Locus of NCL line; and (b) *q*-*p*' plot

It should be noted that the critical state friction angle is expected to be unaffected by the strain rate, as suggested by numerous experimental studies (e.g., [30]), whereas the normal consolidation line (*NCL*) of clays in the v-ln (p') space moves upward with an increase in strain rate (NCL^*). This shift of the *NCL* with increasing strain rate has been observed by many researchers (e.g., [31]-[33]). For undrained conditions, no volume change is allowed so that the specific volume v_i should be constant and must lie on the same unloading-reloading line. Therefore, the updated preconsolidation pressure $p_c'^*$ due to strain rate increase must be at the intersection of NCL^* and the overconsolidation line. Consequently, the upward shift of the *NCL* as a function of strain rate corresponds to an increase in the preconsolidation pressure [34] or overconsolidation ratio (*OCR*) [35], and implies that the soil becomes more dilatant and exhibits larger stiffness and peak undrained shear strength, as observed in reality. The increase in *OCR* adds to the increase in stiffness through the constitutive equations for the plastic modulus and elastic moduli.

To relate the increase in *OCR* and the corresponding preconsolidation pressure to the strain rate increase, Eq. (2) is utilised in this study, along with the theoretical formula that predicts the undrained shear strength based on the MCC model parameters [36]. Consequently, rate-independent plasticity theory is employed to simulate the rate dependent behaviour, avoiding the need to adopt numerically expensive viscoplastic stress-strain integration schemes. Therefore, the adopted model assumes that soil elements at the same initial stress conditions will show different responses if subjected to different strain rates. This is reflected by *OCR* changes and the corresponding enlargements of the yield surface.

Inertial drag force

It seems rational to assume that an inertial drag force exists during penetration of objects into very soft viscous clay, analogous to the hydrodynamic drag experienced by an object passing through water. To show the effect of the drag force on the velocity profile, an inertial drag force is incorporated in the analysis using the following relation

$$F_d = \frac{1}{2} C_d \rho_s A_p V^2 \tag{3}$$

where C_d is the drag coefficient, ρ_s is the density of the soil, A_p is the projected frontal area of the anchor, and V is the current anchor velocity. An approximation of the average drag coefficient equal to 0.7 was suggested by True [37] for a variety of penetrometer geometries and velocities. However, hydrodynamic studies have indicated considerably smaller drag coefficients. Numerical analysis presented by Richardson [38] showed that the drag coefficient C_d decreases with increasing aspect ratio of the penetrometer and ultimately approaches a constant value, which for finless torpedo anchors decreases from 0.35 to a constant value of 0.23 for $L/D \geq 4$, where L and D denote anchor length and diameter, respectively.

Numerical Examples

The numerical framework described previously has been implemented into an in-house FE code, SNAC. This code is employed here to carry out some coupled simulation of dynamic anchors. First, simulation of a model penetrometer is conducted and the analysis results are compared with the corresponding centrifuge data. Then, a series of analyses are performed to study the effect of strain rate on the behaviour of torpedo anchors.

Validation against centrifuge test data

Chow *et al*. [39] reported data from a centrifuge test carried out on a model penetrometer free falling into kaolin clay. The penetrometer had a 60° cone tip and a prototype shaft diameter and length of 1.0 m and 12 m, respectively, and a mass of 28130 kg. The penetrometer achieved impact velocities ranging between 4.7 and 15.6 m/s with corresponding final embedment depths in the range 10.2-16.7 m at prototype scale. The undrained shear strength of the soil $s_u = 1.13z$ kPa was deduced from T-bar penetration tests where z denotes the soil depth in metres. The soil properties are listed in Table 1.

Table 1. Soil parameters

Parameter	Value
Friction angle	$\phi' = 23°$
Slope of normally consolidated line in *e-ln(p')* space	$\lambda = 0.205$
Slope of unloading-reloading line in *e-ln(p')* space	$\kappa = 0.044$
Initial void ratio	$e_0 = 2.14$
Over consolidation ratio	$OCR = 1$
Poisson's ratio	$\upsilon' = 0.3$
Saturated bulk unit weight	$\gamma_{sat} = 17$ kN/m^3
Unit weight of water	$\gamma_w = 10$ kN/m^3
Permeability of soil	$k = 5\times10^{-9}$ m/s

Note: p' is the mean effective stress

Fig. 2 depicts the axisymmetric FE mesh and the corresponding boundary conditions adopted for the numerical simulation. The mesh comprises 3,416 triangular elements and 7,028 nodes.

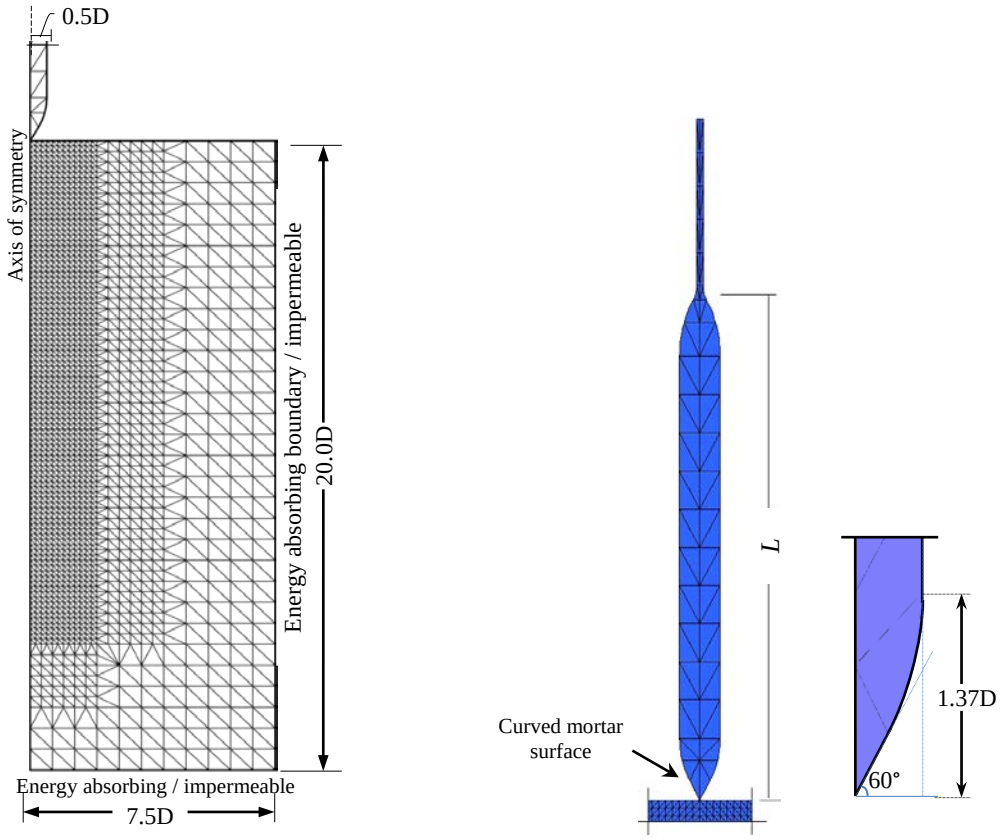

Figure 2. (a) FE model mesh; (b) anchor geometry

The radial thickness of the soil elements underneath the penetrometer is equal to one-third of its shaft radius. Discretisation of the geometry of the penetrometer with quadratic mortar elements facilitates curved surfaces at the cone and top of the anchor (Fig. 2b). Two impact velocities of 4.7 m/s and 6.1m/s were considered in the numerical simulations. The strain rate parameter, the drag coefficient and the friction coefficient at the interface were assumed to be $\eta = 0.2$, $C_d = 0.23$ and $\mu = 0.25$, respectively.

Fig. 3 shows the penetration profile predicted by the numerical analyses and the ultimate penetration depths as measured in the centrifuge test. Good agreement of the ultimate penetration can be observed for the two analyses. The computed anchor tip embedment depths for the impact velocities 4.7m/s and 6.1m/s are, respectively, 10.45m and 12.23m which are only 2.1% and 3% greater than the measured values, providing some experimental validation of the proposed numerical approach and its predictions.

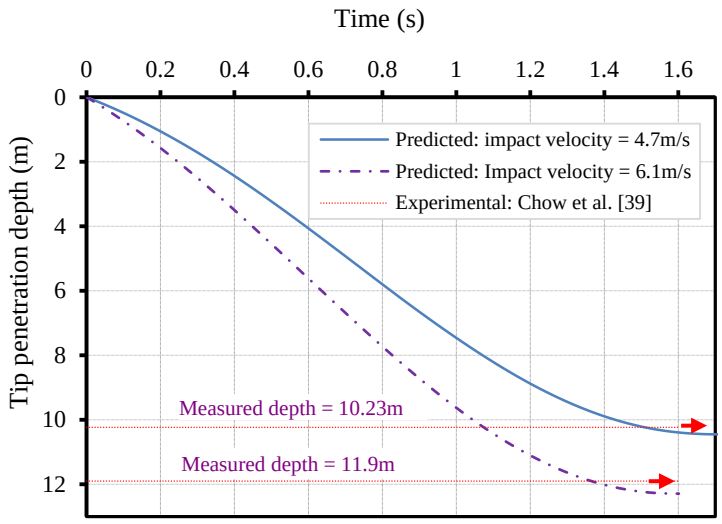

Figure 3. Comparison between numerical prediction and centrifuge test data

Strain rate effect on the behaviour of torpedo anchor

A rigid finless torpedo anchor falling freely into a normally consolidated kaolin clay is analysed in this section. The effect of strain rate on the behaviour of torpedo anchor is then studied in terms of penetration depth, pore pressure generation and frictional resistance. The boundary conditions and geometry of the mesh and torpedo anchor are similar to those adopted in the previous section (Fig. 2), except that the buoyant weight of the anchor is now 150 kN. In order to provide a rather detailed overview of anchor behaviour, two sets of analyses are presented. The first set of simulations assumes a frictionless interface between the soil and anchor so as to study the effects of strain rate only. The second set of analyses incorporates a frictional interface and reveals some practical and important aspects of dynamic anchor behaviour.

Frictionless interface

Fig. 4 depicts the change in the equivalent (apparent) *OCR* value at a penetration depth of 5D for rate parameters of $\eta = 0.15$, and 0.20. The apparent *OCR* value generally increases during penetration and for the rate parameter of $\eta = 0.15$ it reaches a maximum value of 2.7 at some Gauss points, noting that the initial value of *OCR* was 1.0 (Table. 1). The soil elements

within a zone around the cone of the advancing torpedo undergo very high strain rates so that the equivalent value of *OCR* is noticeably increased for that zone. During anchor penetration the shear strain rate varies throughout the soil body in which for soil elements displaced from the tip zone to the anchor shaft the strain rate is alleviated, resulting in decreased magnitudes of the apparent *OCR* along the shaft. However, the final value is still larger than the initial *OCR*. Increasing the strain rate parameter to 0.20, increases the maximum value of apparent *OCR* to 4.1 (Fig. 4b).

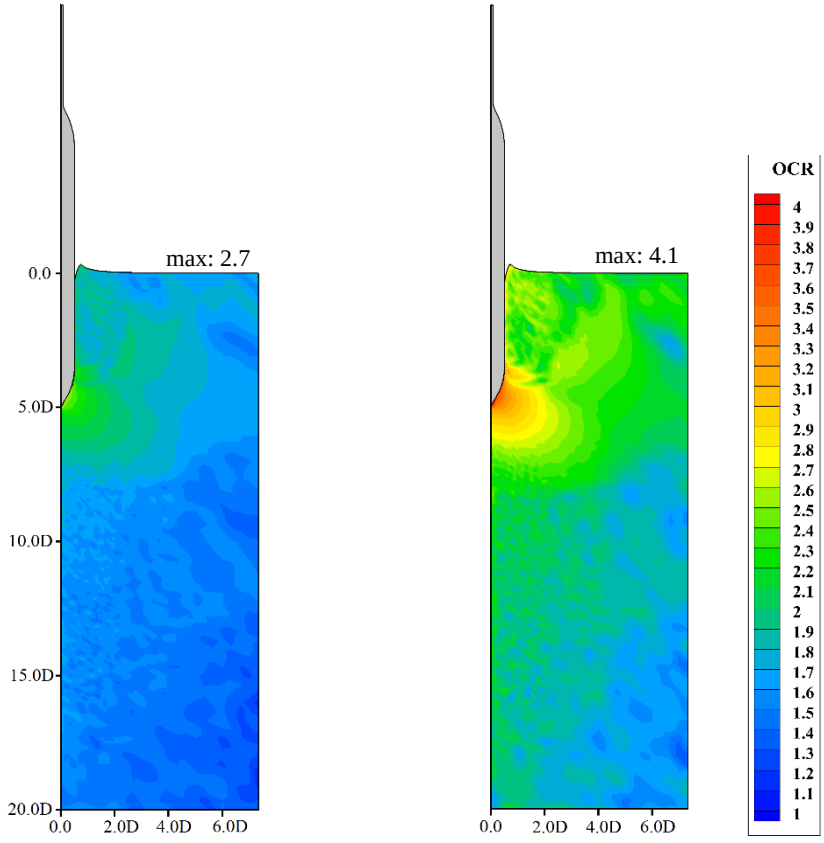

Figure 4. Apparent OCR value evaluated based on the strain rate within the soil body at a penetration depth of 5.0D: (a) η = 0.15; (b) η = 0.20

The soil resistance profile is depicted in Fig. 5 for two values of the rate parameter. It is observed that the total penetration resistance increases for the rate dependent case and the embedment depth is decreased, accordingly. The soil resistance at the end of installation is about 65% larger for the rate dependent case (η = 0.2) compared with the rate-independent one at the same penetration depth.

The embedment depth for the rate independent case is 13.9D whereas it decreases to 8.7D when the rate parameters is 0.20. Therefore, it can be seen that the increases in soil resistance due to strain rate effect is a key factor in the analysis of dynamically penetrating anchors. Although the most of experimental results on free falling anchors have identified the strain rate effect on the ultimate embedment depth, they have not described how strain rate may influence the generation of excess pore pressures and sleeve frictional force. These are explained as follows.

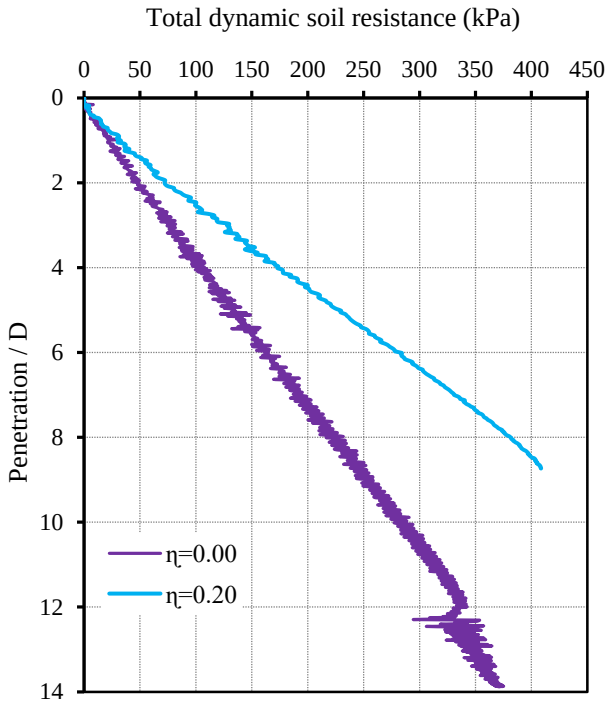

Figure 5. Total dynamic soil resistance profile for different values of rate parameter (η)

Fig. 6 depicts two excess pore pressure contour plots with rate parameters of $\eta = 0.0$ and $\eta = 0.20$. It is seen that, for the rate independent normally consolidated clay (Fig. 6a), a compressive excess pore pressure bulb is typically formed around the anchor tip and shaft. This bulb extends a distance of approximately 4D in the radial direction and about 1D in the vertical direction, as measured from the anchor tip. The maximum compressive values are developed at the anchor tip (~210 kPa) and extend to its shoulder (~160 kPa). Moreover, a tensile region (~-40kPa) is located at a distance of about 2D vertically underneath the anchor tip. This is due to development of plastic expansion (softening) region beneath the pile tip after the compression zone.

A similar plot for the rate dependent case is presented in Fig. 6b. It is observed that a region of suction has been locally created around the cone and also within a thin layer of soil along and adjacent to the anchor shaft. The creation of this suction zone (due to elasto-plastic expansion of soil) is merely a consequence of the high strain rate and the corresponding increase of the apparent *OCR* value. As observed in Fig. 4, soil elements around the conical section experience the highest strain rates and correspondingly much larger values of suction pore pressures (~ -600 kPa) are detected (Fig. 6b). This situation of high strain rates is also combined with the vertical stress relief that happens near the cone shoulder and leads to a more pronounced dilative behaviour of the soil. The normal stress relief may occur at a specific location depending on the geometry of anchor tip implying that the geometry of anchor tip may considerably influence the generation of excess pore pressures. It is also emphasised that the developed suction pore pressures can cause desaturation of the pore pressure measuring systems in experimental tests, and that reliable pore pressure data may not be consistently obtained. Therefore, the finding of a thin zone of suction around the anchor may have important consequences for pore pressure measurements made and interpreted using a conventional cone penetrometer (CPT).

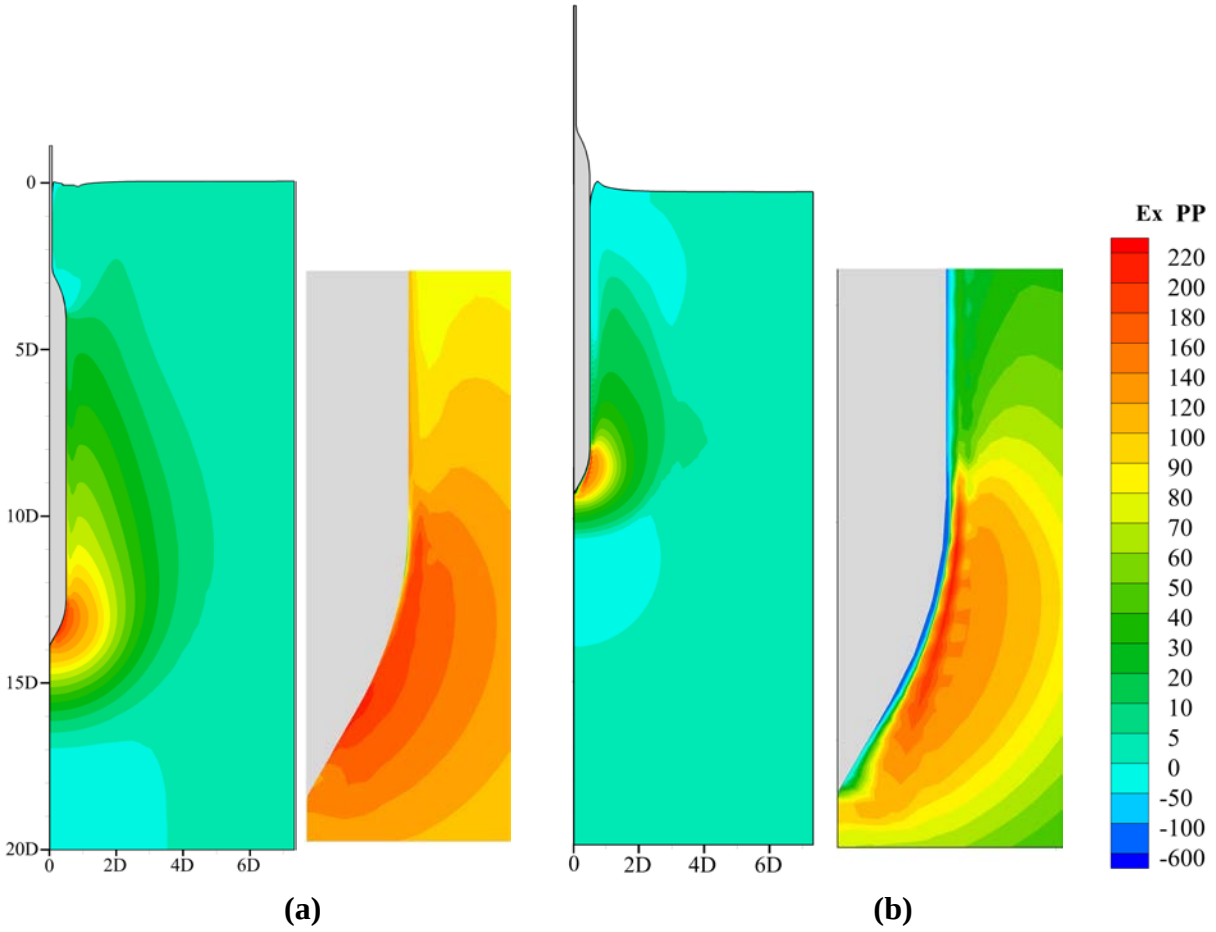

Figure 6. Excess pore pressure (kPa) contour plots: (a) η = 0 and (b) η = 0.2

Frictional interface

It might reasonably be deduced that the tangential frictional force developed at the anchor-soil interface would not be significant because of the undrained behaviour of the soil (*i.e.*, due to the expected lower effective stresses at the interface). However, the numerical results from the previous section revealed that a thin layer of tensile excess pore pressure is actually created along almost the entire length of the torpedo shaft during the installation process. This will increase the effective stresses at the soil-anchor interface and lead to higher frictional forces.

Fig. 7 depicts the soil resistance profile for a rate parameter η = 0.2 with friction coefficients μ = 0 and 0.2. The embedment depth decreases when the friction coefficient is 0.2, as expected. For the frictionless case, the penetration depth is around 9.4D, while it decreases to ~ 7.2D for the frictional case. It is also seen that the frictional soil resistance starts to diverge from the frictionless case at the embedment depth of ~2.7D which is due to the separation of soil and anchor at shallower depths.

Therefore, it is observed that frictional resistance is generated during the fast penetration of dynamic anchors and its effects cannot be ignored.

Conclusions

Numerical analyses have been conducted to evaluate the effect of strain rate on the behaviour of dynamically penetrating anchors. The implications of the strain rate effects on the generation of excess pore pressure and the frictional resistance were specifically studied. It was shown that when the effect of strain rate is taken into account, a zone of suction is typically created around the anchor tip and also within a thin layer of soil along and adjacent to the anchor shaft.

Despite the undrained conditions in the soil, frictional resistance is generated during the fast penetration of dynamically installed anchors. This is largely because of the generation of suction pore pressures and the corresponding increase of the effective stress at the interface between the soil and the anchor. Therefore, it can now be concluded that the strain-rate effects not only increase the bearing resistance, but considerably increase the frictional resistance.

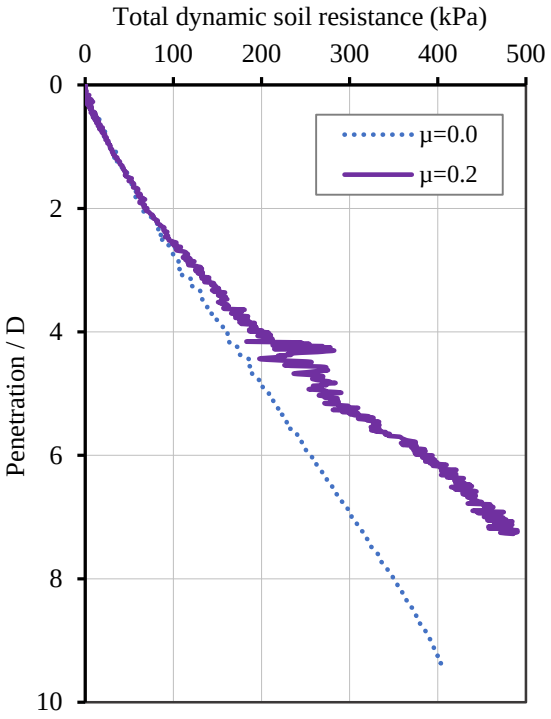

Figure 7. Total dynamic soil resistance profile: μ = 0 & 0.2

References

[1] Graham, J., Crooks, J. H. A. and Bell, L. (1983) Time effects on the stress–strain behaviour of natural soft clays, *Ge'otechnique* **33**(3):327-340

[2] Lefebvre, G. and LeBoeuf, D. (1987) Rate effects and cyclic loading of sensitive clays, *Journal of Geotechnical Engineering* **113**(5):476-489.

[3] Sheahan, T.C., Ladd, C. and Germaine J.T. (1996) Rate dependent undrained shear behaviour of saturated clay, *Journal of Geotechnial and Geoenvironmental Engineering, ASCE* **122**(2):99-108.

[4] Biscontin,G. and Pestana , J. M. (2001) Influence of peripheral velocity on vane shear strength of an artificial clay, *ASTM Geotechnical Testing Journal* **24**(4):423-430.

[5] Lunne, T. and Andersen, K. H. (2007) Soft clay shear strength parameters for deep water geotechnical design, *In: KeynoteAddress, Proc. Sixth Int. Offshore Site Investigation and Geotechnics Conf*, London, UK 51-176.

[6] Nazem, M., Carter, J.P., Airey, D.W. and Chow, S.H. (2012) Dynamic analysis of a smooth penetrometer free-falling into uniform clay, *Geotechnique* **62**(10): 893-905.

[7] Carter, J. P., Nazem, M., Airey, D.W. and Chow, S. H. (2010) Dynamic analysis of free falling penetrometers in soil deposits, *Geotechnical Special Pub. 199. GeoFlorida 2010-Advances in Analysis, Modelling and design, ASCE*, West Palm Beach, Florida 53-68.
[8] Kim, Y. H., Hossain, M. S. aand Wang, D. (2015) Effect of strain rate and strain softening on embedment depth of a torpedo anchor in clay, *Ocean Engineering* **108**(1):704-715.
[9] Sabetamal, H., Nazem, M. and Carter, J. P. (2013) Numerical analysis of Torpedo anchors, *In the proceedings of the 3rd International Symposium on Computational Geomechanics, ComGeo III*, Krakow, Poland 621-632.
[10] Sabetamal, H., Nazem, M., Carter, J. P. and Sloan, S. W. (2014) Large deformation dynamic analysis of saturated porous media with applications to penetration problems, *Computers and Geotechnics* **55**:117–13.
[11] Truesdell, C. and Toupin, R. (1960) The classical field theories, *In Handbuch der Physik, Flugge S (ed.). Springer* Vol. 3.
[12] Morland L. W. (1972) A simple constitutive theory for a fluid-saturated porous solid, *Journal of Geophysical Research* **77**, 890–900.
[13] Sabetamal, H. (2015) Finite Element Algorithms for Dynamic Analysis of Geotechnical Problems, *PhD thesis, The University of Newcastle*, Australia.
[14] van den Berg, P., deBorst, R. and Huetink, H. (1996) An Eulerian finite element model for penetration in layered soil, *International Journal for Numerical and Analytical Methods in Geomechanics* **20**(12) 865-886.
[15] Hu, Y. and Randolph, M.F. (1998) A practical numerical approach for large deformation problems in soil, *International Journal for Numerical and Analytical Methods in Geomechanics* **22**(5) 327-350.
[16] Susila, E. and Hryciw, R.D. (2003) Large displacement FEM modelling of the cone penetration test (CPT) in normally consolidated sand, *International Journal for Numerical and Analytical Methods in Geomechanics* **27**(7) 585-602.
[17] Nazem, M., Sheng, D. and Carter, J.P. (2006) Stress integration and mesh refinement in numerical solutions to large deformations in geomechanics, *International Journal for Numerical Methods in Engineering* **65**,1002**–**1027.
[18] Sulsky, D., Zhou, S. and Schreyer, H.L. (1995) Application of a particle-in-cell method to solid mechanics, *Computer Physics Communications* **87**, 235-252
[19] Beuth, L., Więckowski, Z. and Vermeer, P.A. (2011) Solution of quasi-static large-strain problems by the material point method, *International Journal for Numerical and Analytical Methods in Geomechanics* **35**(13) 1451-1465.
[20] Benson, D.J. (1989) An efficient, accurate, simple ALE method for nonlinear finite element programs, *Computer Methods in Applied Mechanics and engineering* **72**, 305–350.
[21] Wang, D., Bienen, B., Nazem, M., Tian, Y., Zheng, J., Pucker, T. and Randolph, M.F. (2015) Large deformation finite element analyses in geotechnical engineering, *Computers and Geotechnics* **65**, 104-114.
[22] Fressmann, D. and Wriggers. P. (2007) Advection approaches for single- and multi-material arbitrary Lagrangian–Eulerian finite element procedures, *Computational Mechanics* **39**, 153-190.
[23] Hallquist, J. O., Goudreau, G. L. and Benson, D. J. (1985) Sliding interfaces with contact impact in large-scale Lagrangian computations, *Computer Methods in Applied Mechanics and Engineering* 107-137.
[24] Wriggers, P. and Simo, J. C. (1985) A note on tangent stiffness for fully nonlinear contact problems, *Communications in Applied Numerical Methods* **1**,199-203.
[25] Fischer, K. A. and Wriggers. P. (2005) Frictionless 2D contact formulations for finite deformations based on the mortar method, *Computational Mechanics* 36, 226-244.
[26] Sabetamal, H., Nazem, M., Sloan, S. W. and Carter, J. P. (2016) Frictionless contact formulation for dynamic analysis of nonlinear saturated porous media based on the mortar method, *International Journal for Numerical and Analytical Methods in Geomechanics* **40**(1) 25-61
[27] Casagrande, A. and Wilson, S.D. (1951) Effect of Rate of Loading on the Strength of Clays and Shales at Constant Water Contents, *Geotechnique*, **2**(3)251-263.
[28] Bjerrum, L., Simons, N. and Torblaa, I. (1958) The Effect of Time on the Shear Strength of a Soft Marine Clay, *Proceedings of the Brussels Conference on Earth Pressure Problems*, Vol I, 148-158.
[29] Skempton, A. W. (1948) Vane tests in alluvial plain of the River Forth near Grangemouth, *Geotechnique*, **1**, 111-124.
[30] Mitchell, J. K. and Soga, K. (2005) Fundamentals of soil behaviour, *3rd ed. New York: Wiley Inter-Science.*
[31] Bjerrum, L. (1967). Engineering geology of Norwegian normally consolidated marine clays as related to settlements of buildings, *Géotechnique* **17**(2):81-118.
[32] Leroueil, S., Kabbaj, M., Tavenas, F. and Bouchard, R. (1985) Stress-strain rate relation for the compressibility of sensitive natural clays, *Géotechnique* **35**(2), 159-180.
[33] Sheahan, T. C. (2005) A soil structure index to predict rate dependence of stress–strain behavior, *In: Testing, modeling and simulation in geomechanics, ASCE, Geotechnical Special Publication* **143**, 81-97.
[34] Silvestri, V., Yong, R. N., Soulie, M. and Gabriel, F. (1986) Controlledstrain, controlled-gradient and standard consolidation testing of sensitive clays, *In: Yong RN, Townsend FC (eds) Proceedings of consolidation of soils: testing and evaluation: a symposium, issue 892, ASTM Committee D-18 on Soil and Rock* , 433-450.
[35] Katti, D. R., Tang, J. P. and Yazdani, S. (2003) Undrained Response of Clays to Varying Strain Rate, *Journal of Geotechnical and Geoenvirontal Engineering* **129**(3) 278-282.
[36] Potts, D. M. and Zdravkovic, L. (1999) Finite element analysis in geotechnical engineering: theory. *Thomas Telford, London.*
[37] True, D. G. (1976) Undrained Vertical Penetration into Ocean Bottom Soils, *PhD Dissertation, University of California, Berkeley, California.*

[38] Richardson, M. D. (2008) Dynamically installed anchors for floating offshore structures, *Ph.D. thesis, University of Western Australia.*
[39] Chow, S. H., O'Loughlin, C.D. and Randolph, M. F. (2014) Soil strength estimation and pore pressure dissipation for free-fall piezocone in clay, *Géotechnique* **64**(10):817–824.